Applied Catalysis B: Environmental 179 (2015) 521–529

Contents lists available at ScienceDirect

Applied Catalysis B: Environmental

journal homepage: www.elsevier.com/locate/apcatb

Low-temperature CO oxidation by transition metal polycation exchanged low-silica faujasites

O.P. Tkachenko[a], A.A. Greish[a], A.V. Kucherov[a], K.C. Weston[b], A.M. Tsybulevski[b,*], L.M. Kustov[a,c]

[a] N.D. Zelinsky Institute of Organic Chemistry RAS, Leninsky Prospect, 47, Moscow 119991, Russia
[b] Zeochem LLC, 1600 West Hill Street, Louisville, KY 40210, USA
[c] Chemistry Department of Moscow State University, Leninskie Gory 1, 3, 119991 Moscow, Russia

ARTICLE INFO

Article history:
Received 18 November 2014
Received in revised form 12 April 2015
Accepted 16 April 2015
Available online 17 April 2015

Keywords:
Polycations
Transition metals
Zeolites
Faujasite
CO oxidation
Kinetics
Mechanism

ABSTRACT

The kinetics and mechanism of low-temperature carbon monoxide oxidation by transition metal polycation exchanged low-silica faujasite (LSF) are investigated. Single and double Cu, Zn, and Mn polycation containing samples were prepared by ion exchange with the corresponding salt solutions at the conditions of their partial hydrolysis. Catalytic tests of the prepared samples by the micro reactor method demonstrated an exceptional activity of novel catalysts in CO oxidation. Reaction kinetics measurements at gradientless conditions along with the catalysts ESR characterization and DRIFT spectroscopy of chemisorbed CO allowed to single out three different models of CO oxidation over the studied catalysts: a) the Eley–Rideal mechanism for single Zn-, Mn- and double MnCu-polycation exchanged LSF having the zero order of the reaction rate for CO and the first order for O_2; b) the Mars–van Krevelen mechanism for the CuCaLSF catalyst with the reaction rate order 0.11 for CO and the zero order for oxygen; c) the autocatalytic model for CuZn-polycation exchanged faujasite that is characterized by the zero order for both reactants, CO and O_2, with a capability for direct oxidation of carbon monoxide not involving free oxygen.

© 2015 Elsevier B.V. All rights reserved.

1. Introduction

Carbon monoxide oxidation at low, predominantly ambient temperatures of 0–50 °C has been well known since WW I due to its application in combat and commercial gas masks, catalytic filters for indoor air cleaning, and most recently for automotive exhaust gas converters, fuel cells, and CO_2 lasers. Meanwhile, contemporary requirements for an extremely high catalytic activity led to the development and wide implementation of noble metal based catalysts, particularly gold, platinum, and palladium supported on oxides carrier [1–3]. At the same time, the high cost of precious metals has encouraged extensive research efforts for alternative catalytic compositions having comparable catalytic activity [4–6]. Among potential substitutes for noble metal low-temperature CO oxidation catalysts, transition metal (TrM) polycation exchanged zeolites [7–9] attract a particular interest.

TrM polycations in such zeolite structures form nanoclusters of 4–15 Å size with the general formula $[TrM_\alpha O_\beta]^{n+}$, where α varies from 2 to 8, β varies from 0 to 4, and n varies from 2 to 6. Most likely owing to this feature, TrM polycation exchanged zeolites recently demonstrated a remarkable catalytic activity in various reactions [10–13]. In respect to CO oxidation, a superior redox activity of TrM oxide nanoclusters [14] and in particular an excess of oxygen in polycations [15,16] might be largely responsible for the corresponding catalytic activity. It was shown [17,18] that TrM super oxides, especially copper super oxides, can be considered a natural accumulator of excessive slightly bound oxygen providing the CO oxidation activity.

In such a manner, this work was carried out not only with the hope of finding a novel class of efficient catalysts for carbon monoxide oxidation but also to reveal the nature of the catalytic activity of TrM polycation exchanged faujasites in the targeted reaction.

2. Experimental

With the purpose at hand, several samples of Zn-, Mn-, and Cu-polycation exchanged LSF were prepared and tested for activity in CO oxidation along with the characterization by electron

* Corresponding author. Current address: 3010 Kipling Way, Louisville, KY 40205, USA. Tel.: +7 502 473 7442.
E-mail address: amtky@att.net (A.M. Tsybulevski).

http://dx.doi.org/10.1016/j.apcatb.2015.04.029
0926-3373/© 2015 Elsevier B.V. All rights reserved.

paramagnetic resonance (ESR) and CO chemisorption study by diffuse reflectance Fourier transform infrared (DRIFT) spectroscopy.

2.1. Samples preparation

All samples for this study were prepared on the basis of low-silica faujasite (LSF) with Si/Al ratio equal to 1.01 that was selected due to its high cation exchange capacity, which is in turn required for obtaining the ultimate concentration of TrM nanoclusters in the catalyst composition. The samples preparation procedure for the majority of single and double TrM polycation exchanged LSF is described in [13,19]. As an example of the employed procedure of the catalysts preparation, the methodology of $(Cu)_pCaLSF$ sample fabrication is given below in greater detail.

The original material, beaded sodium-potassium form of low-silica faujasite (LSF) was obtained from Zeochem. NaKLSF was first converted into calcium form. For this purpose, 100 g of zeolite beads were treated with 1 L of 1 N solution of calcium chloride at ambient temperature, pH 6.5–7.0 and continuous agitation over 3 h. After washing the Ca-exchanged zeolite with 25 L of deionized water(DIW), the obtained product was treated with 1.25 L of 1 N copper chloride solution at room temperature over 4 h keeping pH of the exchanged solution in the range of 5.0–5.4 by means of 0.05 M buffer solution of basic sodium dihydrophosphate (NaH_2PO_4). The exchanged product was then washed with DIW, dried at 110 °C for 3–4 h and calcined at 250 °C for 2 h.

Formation of the copper cluster polycations from hydrolyzed mononuclear cations can be expressed by the following reactions:

$$2[Cu(OH)]^+ \rightarrow [Cu_2O]^{2+} + H_2O \quad (1)$$

$$[Cu(OH)]^+ + Cu^{2+} \rightarrow [Cu_2O]^{2+} + H^+ \quad (2)$$

Alternatively, polycations of $[Cu]^{2+}$ type may be formed by the condensation reaction of mononuclear metal ions with zero-valent metal atoms as follows:

$$Cu^{2+} + Cu^0 \rightarrow [(Cu2]^{2+} \quad (3)$$

The simultaneous occurrence of the Reactions (1)–(3) and the consecutive evolution of the Reactions (2) or (3) leads to the formation of cluster polycations of the above mentioned general formula $[TrM_\alpha O_\beta]^{2+}$.

In addition to Zn polycation LSF [19], with a view of comparing activities of mono- and polycation exchanged zeolites, a conventional monocation ZnLSF catalyst was prepared. As this took place, to avoid Zn cation hydrolysis, pH of the exchanged $ZnCl_2$ water solution was maintained in the range of 4.9–5.1.

Furthermore, aiming at clarification of the effect of the TrM polycations proportion in double TrM exchanged catalysts, the $(Cu)_p(Zn)_p$LSF-2 [19] sample having the Cu:Zn polycation ratio on the level of 2.0 was supplemented by the sample of $(Cu)_p(Zn)_p$LSF-4 with Cu:Zn ≈4.0. As this is the case, 100 g of the $(Cu)_p$CaLSF sample, which is obtained above, was treated by 1 L of 0.4 N water solution of zinc chloride keeping pH at the level of 5.6–6.0 by 0.08 M water solution of K_2HPO_4.

The cation composition in the prepared samples according to inductively coupled plasma atomic emission spectroscopy (ICP) is given in Table 1. As it can be seen, the sum of all cation equivalents incorporated into TrM polycation exchanged samples significantly exceeds 100% at the rate of monocation. Indeed, it is a usual feature of polycation exchanged zeolites [7,8,13]. Accordingly, the achieved exchange degrees for TrM are distributed in Table 1 between mono- and polycations whereupon the content of the latter is determined as a surplus of the total cation exchange degree of the obtained zeolite sample. In so doing, the polycation contents for CuZn- and CuMn-exchanged samples are calculated in proportion to the corresponding monocation exchange degrees as it was done previously in [13]. The presence of polycations in the sample is indicated by the subscript "*p*" following the corresponding cation symbol in the sample index mark.

In so far as the ion exchange procedure by TrM water solutions can cause partial amorphization of zeolites [20], XRD of the obtained samples is employed for checking the indestructibility of TrM polycation exchanged LSF. Crystallinity of the samples is valued by the cumulative intensity of 16 most intensive peaks on the X-ray pattern. In so doing, monocation ZnLSF serves as a standard with a conditional crystallinity of 100%. The total intensity of 16 peaks for ZnLSF XRD makes up to 121% from the similar value for the original NaKLSF sample.

As it can be seen from Table 1 data, the crystallinity of polycation exchanged LSF is generally on a quite satisfactory level. Some destruction of the crystalline structure is detected for single and double Zn and CuZn polycation exchanged zeolites, however it cannot substantially affect the catalytic activity of the samples. It is also indicative that the general surface area of the catalysts, which was measured by nitrogen adsorption at −196 °C, does not depend on cation composition of the polycation exchanged zeolites and remains unchanged in the 520–565 m^2/g limits.

2.2. Catalysts characterization: ESR measurements

Many of the used in the present study single and double TrM polycation exchanged LSF catalysts were characterized in [13] by X-ray absorption near edge spectroscopy (XANES), electron paramagnetic resonance (ESR) and diffuse reflectance Fourier transform infrared (DRIFT) spectroscopy. In addition, aiming at differentiation of the Cu cations state in the Cu-containing samples, ESR spectra of $(Cu)_pCaLSF$, $(Cu)_p(Mn)_pLSF$, $(Cu)_p(Zn)_pLSF$-2 and $(Cu)_p(Zn)_pLSF$-4 were taken in the X-band ($\lambda \cong 3.2$ cm) at 20 °C and −196 °C on a reflecting spectrometer of the Special Design Bureau of Analytical Instrumentation at the Russian Academy of Sciences that was equipped with a cavity 4104OR with a co-axial quartz Dewar vessel. The ESR signals were registered at the lack of signal saturation at modulation of 5 G in the field range of 2300–3800 G. DPPH was used as a field lebel. Low-loaded sample 0.5%Cu/HY was used as a Cu^{2+} reference standard. Evaluation of amount of ESR-visible Cu(II) was done by comparison of double-integrals of spectra obtained.

As-received samples (0.1–0.3 mm fraction; ∼100 mg) were placed in identical glass ampules (3.0 mm diameter) for ESR measurements and treated consecutively in identical conditions. (1) Ampules were connected with a vacuum system and dried by evacuation for 15 min (∼0.03 Torr) at 90 °C to remove physically adsorbed water; (2) samples were heated for 15 min at 200 °C and evacuated; (3) samples were calcined at 400 °C for 2–15 min and evacuated to remove oxygen and residual water, and sealed off using a gas torch. The ESR spectra were registered at the same magnification at 20 °C after every treatment step, finally ampules were open to air, and ESR measurements were repeated for detection of possible changes of ESR signals due to interaction between gas-phase O_2 molecules and Cu^{2+} ions.

2.3. Catalytic testing

The rates of carbon monoxide oxidation were measured using a micro reactor in a pulse chromatography mode at 25 °C. All samples were crushed to have the grain size of 0.25–0.5 mm. Diameter of the micro reactor was 4 mm. The catalyst portion was 1 g. The carrier gas–dry air. The flow rate – 2.0 mL/s. The CO dose volume – 0.1 mL. The reaction rate constants were determined on the basis of the CO to CO_2 conversion degrees.

With the object of comparative appraisal of new catalysts, the activity of hopcalyte CO oxidation catalyst was measured at

Table 1
Cation composition and crystallinity of the catalyst samples.

Samples	Crystallinity, %	Ion exchange degree, % equiv.								
		Zn		Mn		Cu		Na	K	Ca
		Mono	Poly	Mono	Poly	Mono	Poly			
ZnLSF	100	68	0	–	–	–	–	25	4	–
$(Zn)_pLSF$	89	77	4.9	–	–	–	–	27	4	2
$(Mn)_pLSF$	96	–	–	71	5.5	–	–	33	6	1
$(Cu)_pCaLSF$	92	–	–	–	–	74	12	9.5	9	24
$(Cu)_p(Mn)_pLSF$	93	–	–	33	5.0	62	9.4	8	0.8	25
$(Cu)_p(Zn)_pLSF-2$	86	21.7	2.1	–	–	54.3	4.3	19.8	3.8	12.9
$(Cu)_p(Zn)_pLSF-4$	81	13.3	1.9	–	–	68.5	7.5	23	1.1	12.8

similar conditions. The standard Carulite 300 ($CuMnO_x$) sample was obtained from Carus Corp.

In order to verify the catalyst performance at the CO high conversion degrees and the real conditions of the commercial operation, the dynamic test was carried out employing a thermostatically-controlled glass tube reactor of 25 mm diameter and catalyst bed volume of 45 cm^3. The most active $(Cu)_p(Zn)_pLSF-2$ catalyst beaded with 16% attapulgite binder of 1.4–1.6 mm size was used. Gas composition was: CO – 0.5, CO_2 – 4.5, O_2 – 20, N_2 – 75% v., dry and with the relative humidity (RH) of 50%. Gas flow rate – 1.5 l/min or LHSV – 2000 h^{-1}. Temperature –20 and 50 °C. Gas samples outlet reactor were taken out every 5 min and analyzed by means of a GC with TCD. The required residual CO concentration in the purified flow was set at 5 ppm level. After carbon monoxide breakthrough the run was interrupted and the catalyst was regenerated from adsorbed water in a dry air flow at 320 °C over 4 h. Then the catalyst bed was chilled to the ambient temperature and CO conversion runs were repeated 10 times. In such a manner, the catalyst's ability to completely remove CO from gas flow, its resistance to water vapor and carbon dioxide poisoning and thermal regenerability were determined.

Kinetics of CO oxidation was measured over 3 polycation catalysts: $(Cu)_pCaLSF$, $(Cu)_p(Mn)_pLSF$, $(Cu)_p(Zn)_pLSF-2$ by means of a differential recycle reactor [21] of 20 mm diameter with the catalyst volume of 10 cm^3 at 20 °C. The recycle ratio was maintained on the level >25 so that the CO conversion degree did not exceed 5% mol. Using helium as a carrier gas, two series of experiments were carried out: 1) at a constant CO concentration of 1.0% mol and varied O_2 concentrations in the 0.1–1.0 limits; 2) at a O_2 constant concentration 1.0% mol and varied CO concentrations in the same limits.

2.4. DRIFT study of CO chemisorption

Adsorption of carbon monoxide over selected polycation containing samples was studied by measuring DRIFT spectra using a Nicolet "Protégé" 460 spectrometer equipped with a diffuse reflectance attachment. As it took place, the measurements were carried out at room temperature and equilibrium pressure of 10 and 20 torr. The assessment of spectra is performed by using the OMNIC program. The intensity of IR absorption bands is expressed in Kubelka–Munk units [22,23].

The experimental procedure for the measurements included the following sequence of steps: 1) sample evacuation; 2) thermal treatment at 350 °C for 2 h; 3) spectrum registration; 4) CO letting in; 5) spectrum recording; 6) sample exposure in CO medium for 17 h; 7) spectrum registration; 8) the second exposure in CO for 1 day (+24 h); 9) another spectrum recording; 10) additional sample exposure for 48 h; 11) recording the spectrum again; 12) air admission with spectrum recording; 13) sample exposure to a CO + air mixture overnight (17 h) and spectrum measurement; 14) sample evacuation at room temperature for 2 h and final spectrum registration.

3. Results and discussions

3.1. Catalysts activity

Activities of the studied samples are compared in Table 2.

An essential preeminence of practically all TrM polycation exchanged faujasites over the standard hopcalyte catalyst is the most profound feature among the obtained results. At the similar chemical composition of hopcalyte and $(Cu)_p(Mn)_pLSF$, the results clearly support the significance of TrM nanosized structure for the catalyst activity [24].

The second surprising fact in Table 2 is that among double TrM polycation-containing catalysts, the activity of CuCa- and CuZn-faujasites is appreciably higher than the activity of CuMn-sample. The importance of the Cu:Zn polycation ratio in the catalyst composition for its catalytic performance in CO oxidation should also be pointed out. Similarly, as it was found for the massive co-precipitated CuZn-oxide catalysts [25], the ratio value of 2 appears to be the magic number for providing the ultimate catalytic activity for CuZn-polycation exchanged faujasites too.

3.2. Catalyst efficacy at purification of humid flows and its regenerability

The use of low-silica faujasite as an active component of the catalyst cannot prevent significant co-adsorption of water vapors at humid flows purification and therefore assumes periodic regeneration of the catalyst and a batch operation of the corresponding purification units. Accordingly, along with the catalytic activity, the catalyst performance at CO high conversion degrees, its resistance to poisoning by moisture and ability to reproduce original activity in CO oxidation after adsorbed water desorption are the most important characteristics that define the product's commercial efficacy.

The data in Table 3 confirm that the catalyst $(Cu)_p(Zn)_pLSF-2$ completely matches all the conceivable, most stringent requirements for various commercial applications. First of all, the

Table 2
Activities of the catalysts in CO oxidation.

Catalyst	Rate constant,newline mol/g bar s 10^3
Hopcalyte	0.75
ZnLSF	0.76
$(Zn)_pLSF$	1.20
$(Mn)_pLSF$	0.72
$(Cu)_pCaLSF$	3.8
$(Cu)_p(Mn)_pLSF$	2.9
$(Cu)_p(Zn)_pLSF-4$	3.2
$(Cu)_p(Zn)_pLSF-2$	8.4

Table 3
Carbon monoxide removal from gas flow by $(Cu)_p(Zn)_pLSF$-2 catalyst.

Catalyst state	Time Before CO breakthrough, hours			
	Temperature, °C			
	20		50	
	Dry gas	RH-50%	Dry gas	RH-50%
Fresh	>16 h	4 h 20 min	>16 h	11 h 35 min
After 10 cycles adsorption- regeneration	N/A	4 h 05 min	N/D	

Initial CO – 0.5% v., Breakthrough – 5 ppmv; RHSV – 2000 h^{-1}.

capability of the catalyst to provide >99.9% CO conversion degree at relatively short contact time (<2 s) should be pointed out. Secondly, the relatively small portion of the catalyst provides carbon monoxide removal from gas flow even at the most favorable conditions for moisture pick-up, i.e., the relative humidity of 50% and temperature of 20 °C. As this takes place, the moisture adsorption by the catalyst before CO breakthrough reaches ~10% w., which comprises almost 45% from its equilibrium water capacity. This exceptional feature of the catalyst performance shows that the competitive water vapor adsorption has nothing to do with the catalyst active sites deactivation, and CO breakthrough proceeds only when the catalyst mass transfer system is completely occupied by the adsorbed moisture.

It is also indicative that the catalyst does not give a rise to any signs of deactivation at a dry gas flow purification, and elevation of the run temperature to 50 °C leads to a significant increase of the catalyst operation time before CO breakthrough. Thus, a desiccant bed addition in the front of the suggested catalyst may provide a continuous, uninterrupted operation of the gas purification unit. Similarly, it is reasonable to expect a continuous operation of the catalyst at the thermal conditions that exclude an appreciable water pick-up, most likely at the temperatures higher than 70–90 °C.

The thermal regeneration of the catalyst from the adsorbed water wholly reproduces the catalyst's original activity. Thus, the data in Table 3 support a high hydrothermal stability of the transition metal polycation exchanged faujasites that was manifested earlier in [11,13].

Finally, Table 3 data demonstrate that CO_2 presence in the composition of the gas to be purified does not affect the catalyst performance in CO oxidation even at 9:1 concentration ratio. This fact is in full accordance with the kinetic equations that are presented later, in Section 3.4. The rates of CO oxidation are not decelerated by the reaction product.

3.3. TrM cations distribution by ESR study

The results of the ESR study of the TrM polycation containing samples help to understand the peculiar features of their catalytic behavior. ESR spectra for two Mn-containing catalysts $(Mn)_pLSF$ and $(Cu)_p(Mn)_pLSF$ are compared in Fig. 1. As it is seen in Fig. 1a, the evacuated $(Mn)_pLSF$ sample shows a quite intense ESR signal with traces of a fine structure ($g \sim 2.00$, $\Delta H = 500$ G) being typical of strongly magnetically-interacting Mn^{2+} ions stabilized by the zeolite matrix. The inlet of air does not cause a change of the ESR signal at room temperature (Fig. 1a).

The signal taken at −196 °C after the sample impregnation with water becomes more intense, but no measurable improvement of the fine structure takes place. In other words, liquid water filling zeolite channels does not weaken the mutual interaction between paramagnetic Mn^{2+} ions. Thus, the $(Mn)_pLSF$ sample stabilizes a considerable portion of manganese in the form of magnetically interacting Mn(II) ions. It looks like this part of Mn introduced is not very reactive in respect to O_2 and H_2O.

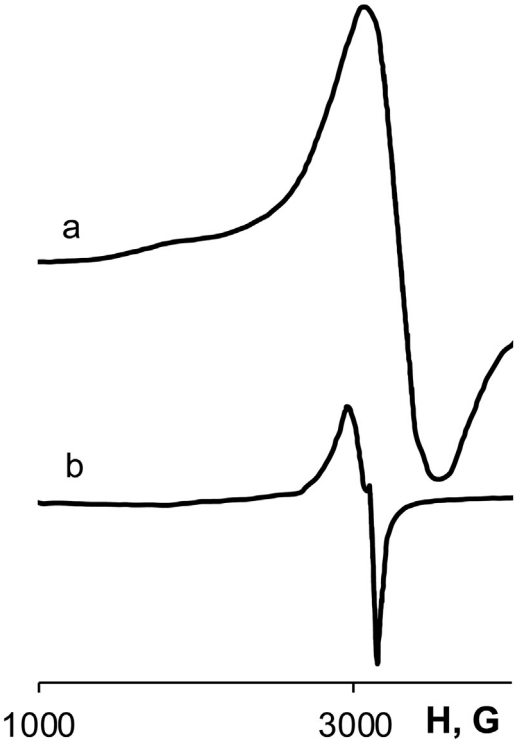

Fig. 1. ESR signals taken at 20 °C: (a) $(Mn)_pLSF$; (b) $(Cu)_p(Mn)_pLSF$.

The evacuated double polycation sample $(Cu)_p(Mn)_pLSF$ shows a quite weak ESR signal (Fig. 1b) of another type: this asymmetric spectrum with traces of a fine structure is typical for interacting Cu^{2+} ions. Surprisingly, even a trace of the superimposed line from Mn^{2+} is not seen in this case (Fig. 1b). So, the introduction of copper drastically changes the distribution of manganese ions. At the same time, an important peculiarity of the copper–manganese system is detected: the comparison of the ESR spectra in Fig. 1 demonstrates a strong influence of Cu on the Mn cations distribution in the zeolite framework. One can suppose that the copper component quantitatively replaces manganese from the sites capable of retaining Mn(II) ions. It would be useful to note here that Mn K edge XANES spectra obtained in [13] for $(Mn)_pLSF$ and $(Cu)_p(Mn)_pLSF$ samples also show that manganese species in both catalysts are found exclusively in the 2+ oxidation state.

Thus, a relatively low catalytic activity of manganese-containing samples $(Mn)_pLSF$ and $(Cu)_p(Mn)_pLSF$ in Table 2 is explained by the low reactivity of Mn and CuMn polycations.

The spectra of other Cu-containing polycation samples $(Cu)_pCaLSF$, $(Cu)_p(Zn)_pLSF$-2 and $(Cu)_p(Zn)_pLSF$-4 are compared in Figs. 2–4. All three samples dried at mild conditions (evacuation at 90 °C) show quite intense asymmetric ESR signals that are typical for magnetically interacting Cu^{2+} ions stabilized in the zeolite matrix as polycationic species without a regular structure. In spite

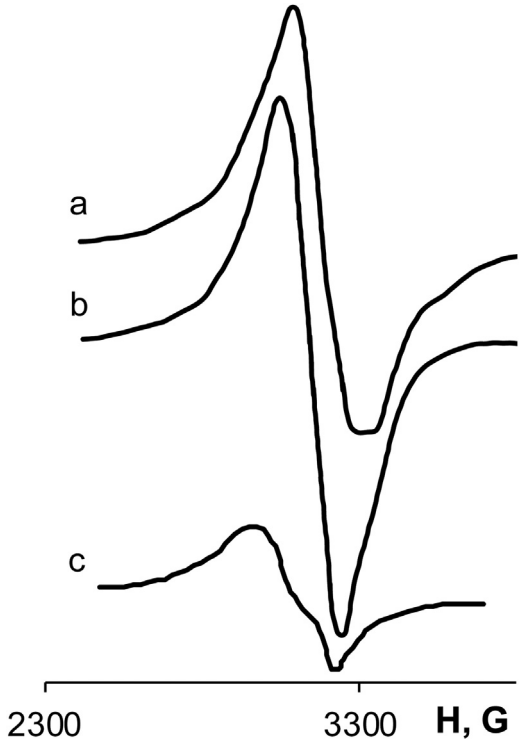

Fig. 2. ESR signals for $(Cu)_pCaLSF$: (a) after evacuation at 90 °C; (b) after heating at 200 °C for 15 min; (c) after calcination at 400 °C for 15 min.

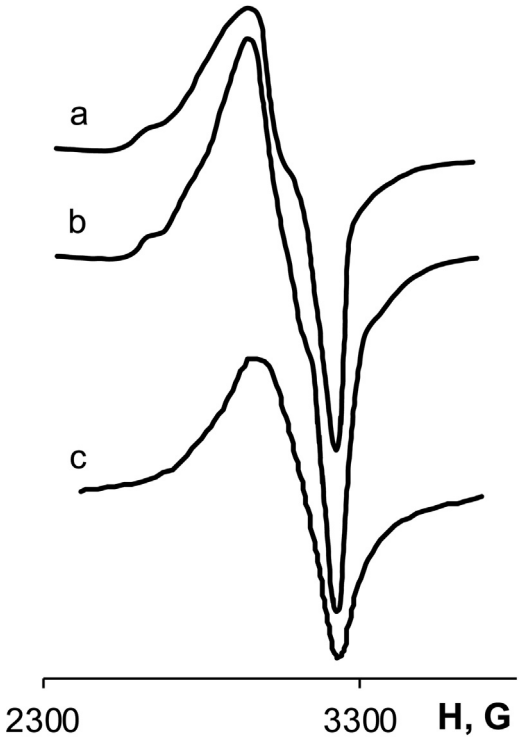

Fig. 3. ESR signals for $(Cu)_p(Zn)_pLSF$-2 at 20 °C: (a) after evacuation at 90 °C; (b) after heating at 200 °C for 15 min; (c) after calcination at 400 °C for 15 min.

of quite low absolute accuracy of ESR measurements (±20%), comparison of these signals with the spectrum of the reference sample 0.5%Cu/HY permits to conclude that the main part of copper(II) ions contributes in signals obtained (Figs. 2 a; 3 a; 4 a). By other words, the main part of copper in abovementioned samples is ESR-visible

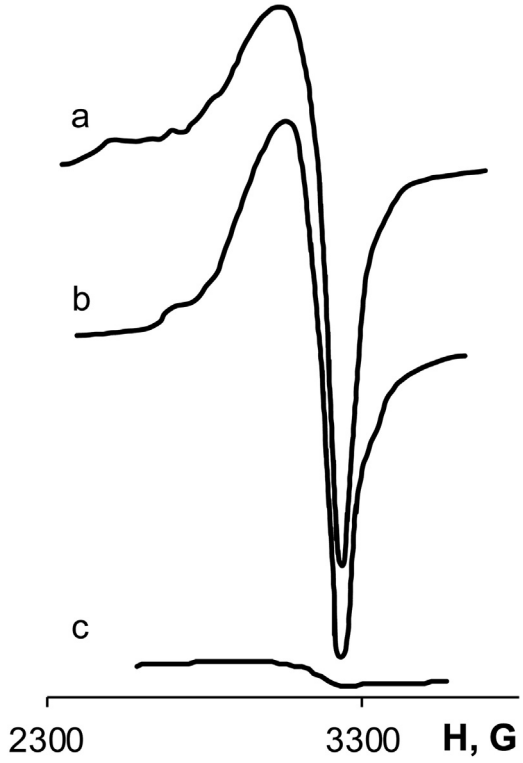

Fig. 4. ESR signals for $(Cu)_p(Zn_p)$LSF-4: at 20 °C (a) after evacuation at 90 °C; (b) after heating at 200 °C for 15 min; (c) after calcination at 400 °C for 2 min.

and ESR data in this case are quite informative. No fine structure appears in ESR spectra of Cu^{2+} after lowering of the recording temperature down to −196 °C being indicative of weak magnetical interaction between paramagnetic cations.

Accordingly, original double polycation-exchanged faujasites contain a lot of water to stabilize a considerable fraction of copper in the form of associated, magnetically-interacting Cu(II) ions. Signals are similar in intensity and differ slightly in shape (Figs. 2 a; 3 a; 4 a), so, the difference in the copper distribution in the starting samples seems to not be pronounced. However, the ESR study of the samples after a step-by-step calcination at elevated temperatures allows one to obtain additional important information.

Thermal treatment of the samples at 200 °C for 15 min does not result in considerable changes of Cu^{2+}-ESR signals (Figs. 2–4). All three samples still contain similar weak associates of copper(II) ions. The inlet of air causes no changes of the ESR signals at room temperature. In other words, paramagnetic O_2 molecules filled the zeolite channels do not exert any influence on the mutual interaction between associated paramagnetic Cu^{2+} ions.

However, a more severe dehydration of the samples at 400 °C allows detecting a significant qualitative difference between the samples studied. Short-term calcination of the sample $(Cu)_p(Zn)_pLSF$-4 (400 °C, 2 min) results in immediate complete disappearance of the Cu^{2+}-ESR signal (Fig. 3c), and the sample changes color from blue to dark gray. It seems that the main part of copper introduced in $(Cu)_p(Zn)_pLSF$-4 can be easily aggregated into ESR-silent copper oxide species with a regular structure due to removal of residual water.

In contrast, two other samples demonstrate a much higher thermal stability against aggregation of copper(II) polycations. The gradual decrease of the Cu^{2+}-ESR signal intensity is quite slow at 400 °C for both $(Cu)_pCaLSF$ and $(Cu)_p(Zn)_pLSF$-2, and even after 15 min of calcination, the samples retain the main part of ESR-visible Cu(II)-species (Figs. 2 c and 3 c). Thus, removal of residual water is not sufficient in this case for the formation of CuO

particles with a regular structure, and the stabilizing effect can be related to the presence of the second cation (Zn, Ca) and formation of double cation aggregates. The lack of a stabilizing effect of Zn in $(Cu)_p(Zn)_p$LSF-4 should be related to the insufficient content of Zn cations in this catalyst composition (see Table 1).

Here is also the main distinction of the $(Cu)_p(Zn)_p$LSF-2 catalyst from its CuMn analog $(Cu)_p(Mn)_p$LSF (Fig. 1), for which a low reactivity of CuMn-polycations was detected. Accordingly, an enhanced catalytic activity of $(Cu)_p$CaLSF and $(Cu)_p(Zn)_p$LSF-2 samples in CO oxidation (Table 2) has to be attributed to the formation of single and double Cu and CuZn polycation clusters in the catalysts composition.

3.4. Kinetics of CO oxidation

The kinetic curves of CO oxidation over three Cu-containing catalysts are presented in Fig. 5.

It is interesting that the most active catalyst among the studied TrM polycation exchanged faujasites, $(Cu)_p(Zn)_p$LSF-2, (Table 2) shows the zero order of CO oxidation rate for both reactants, CO and O_2:

$$r = k{p_{CO}}^0{p_{O_2}}^0 \quad (1)$$

Such unconventional behavior was observed for the gold supported catalyst [26] and was attributed to strong chemisorption of O_2 on the gold metal component and CO over oxide support. Moreover, the zero order of the CO oxidation reaction for both reactants over a non-metal catalyst most likely has been found for the first time in the present study. This feature might be related to the specific structure of double CuZn nanoclusters (see Fig. 3 interpretation in Section 3.3) and to the above-mentioned excess of oxygen in polycations. Unlike $(Cu)_p(Zn)_p$LSF-2, the CO oxidation rates over the $(Cu)_p$CaLSF catalyst are governed by the 0.11 order for the carbon monoxide partial pressure and the zero order for oxygen (Fig. 5):

$$r = k{p_{CO}}^{0.11}{p_{O_2}}^0 \quad (2)$$

Kinetic equations of such a type are usually inherent to the Mars–van Krevelen mechanism [27] that involves the interaction of chemisorbed CO with oxygen atoms of oxide lattice with the following reproduction of the latter by gas phase O_2 [28,29]. Finally, double TrM polycation exchanged $(Cu)_p(Mn)_p$LSF, as it is shown in Fig. 5, presents the third different mechanism of CO oxidation with the kinetics of the first order for O_2 and the zero order for the CO partial pressure:

$$r = k{p_{CO}}^0{p_{O_2}}^{1.0} \quad (3)$$

Similar kinetic regularities were observed for the noble metal catalysts [30,31]. Indeed, noble metals can strongly adsorb carbon monoxide, even sometimes being considered as a CO trapper [32]. In such a manner, the reaction kinetics of type (3) is typically related to the classic Eley–Rideal mechanism with CO chemisorption and retention on metal centers and its following interaction with gas phase oxygen molecules [30,33]. As it was revealed by the ESR study, Cu^{2+} cations in $(Cu)_p(Mn)_p$LSF displace Mn^{2+} from strong cation positions so that CuMn faujasite as opposed to CuZn and CuCa polycation analogs is not tied with double CuMn aggregates formation and consequently is not capable of delivering oxygen for the Mars–van Kravelen mechanism of CO oxidation. In such a manner, in this case, the reaction likely proceeds through CO chemisorption on Cu^{2+} cations.

3.5. CO chemisorption and oxidation mechanism according to DRIFT study

The DRIFT spectra for CO adsorbed by the two Zn-exchanged faujasites, monocation ZnLSF and polycation $(Zn)_p$LSF are compared in Fig. 6, for Mn-containing samples $(Mn)_p$LSF and $(Cu)_p(Mn)_p$LSF in Fig. 7, while spectra for CO chemisorption on $(Cu)_p$CaLSF and $(Cu)_p(Zn)_p$LSF-2 catalysts are presented in Figs. 8 and 9, respectively.

As it can be seen in Fig. 6, the spectra for both mono- and polycation Zn-exchanged faujasites are very similar. Three bands of weak intensity at 2128, 2165, and 2200 cm^{-1} appear in the spectra after CO adsorption. It is quite probable that these stretching vibrations reflect the formation of various types of carbonyls resulting from CO chemisorption on Zn^{2+} cations, though the remaining Na cations may contribute to the low-frequency shoulder [34]. At the same time, it should be taken into account in the further consideration of the DRIFT spectra of CO adsorbed by TrM polycation exchanged faujasites that the contents of alkali and alkali-earth metal cations in all the samples are about the same and much lower than the content of the transition metal cations. The scale of the intensities of the CO bands for the Zn-containing samples (Fig. 6) is roughly 0.05 Kubelka–Munk units. So the intensities of the bands that might be ascribed to CO complexes with Na, K, and Ca must be lower than this value. Comparison of the scales of the intensities of the CO bands in Figs. 6–9, shows that the intensities of the CO bands and an order of magnitude for Mn-, Cu-, CuMn- and CuZn-containing samples (Fig. 7–9) are appreciably higher than for Zn mono- and polycation exchanged samples in Fig. 6. Thus, it leads to the conclusion that CO adsorption on alkali and alkali-earth metal cations makes a negligible contribution in the obtained spectral patterns and may be ignored.

Noteworthy Zn polycations do not affect CO chemisorption on the $(Zn)_p$LSF sample. It is also peculiar for both Zn-exchanged faujasites that their exposure in a CO atmosphere over 89 h does not

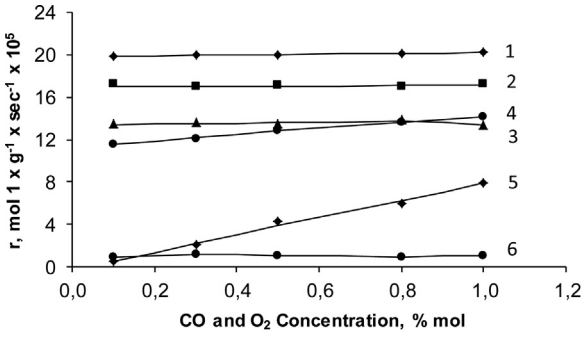

Fig. 5. Carbon monoxide oxidation rates as a function of CO and O_2 concentration: lines 1, 3, 6 – CO; lines 2, 4, 5 – O_2

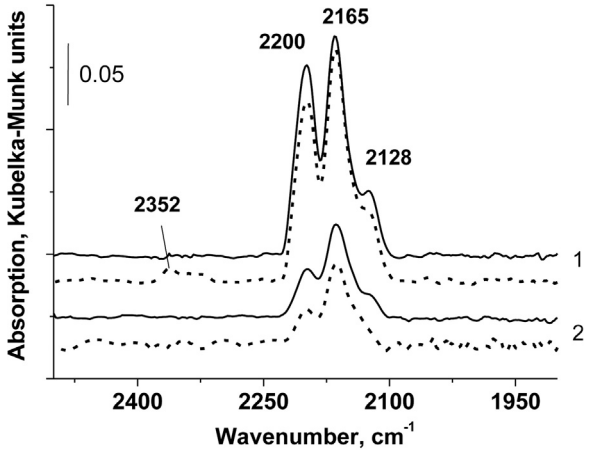

Fig. 6. DRIFT spectra of CO adsorbed on ZnLSF (1) and $(Zn)_p$LSF (2) catalysts: solid curve – 10 min; dotted curve – 89 h.

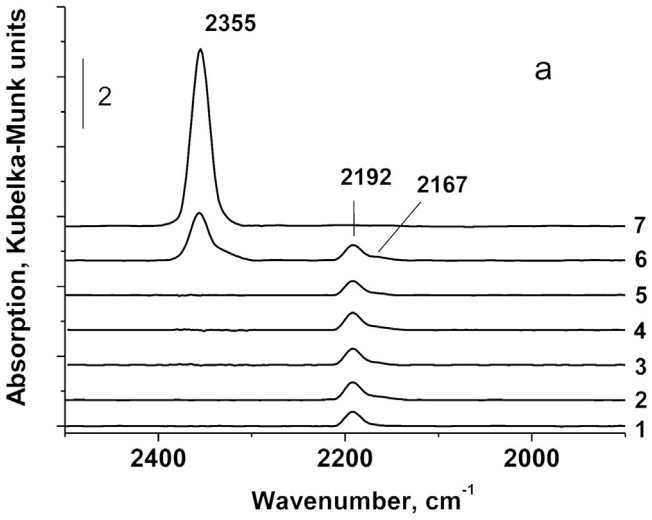

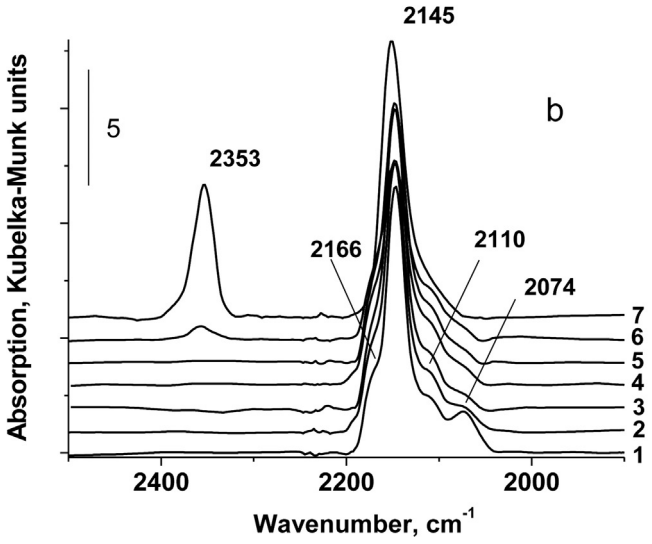

Fig. 7. DRIFT spectra of CO adsorbed on $(Mn)_pLSF$ (a) and $(Cu)_p(Mn)_pLSF$ (b) samples: 1–10 min; 2–2 h; 3–20 h; 4–27 h; 5–93 h; 6 – + air, 10 min; 7–2 h.

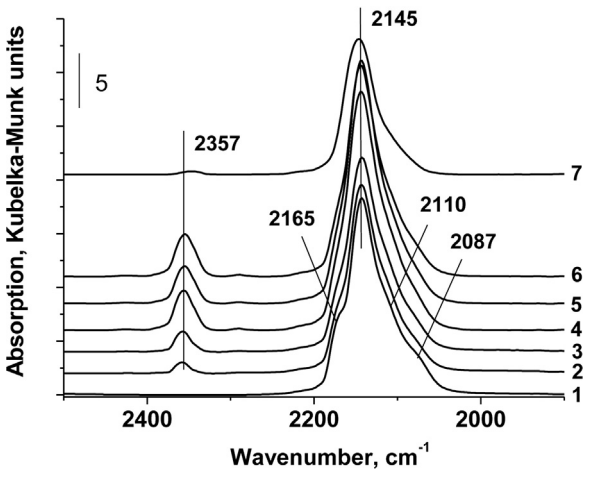

Fig. 8. DRIFT spectra of CO chemisorbed on the $(Cu)_pCaLSF$ catalyst: 1–10 min; 2–17 h; 3–41 h; 4–89 h; 5 – + air, 10 min; 6–17 h; 7–vacuum, 2 h.

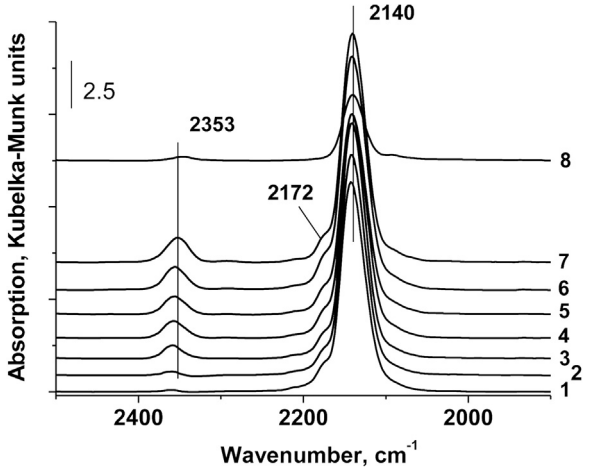

Fig. 9. DRIFT spectra of CO chemisorbed on the $(Cu)_p(Zn)_pLSF$-2 catalyst: 1–10 min; 2–2 h; 3–20 h; 4–44 h; 5–68 h; 6 – + air, 10 min; 7–17 h; 8–vacuum, 2 h.

cause any perceptible changes in the spectra. The band of adsorbed CO_2 at 2352 cm^{-1} appears only after air admission to the samples.

CO adsorption at ambient temperature and equilibrium pressure of 10 Torr on evacuated $(Mn)_pLSF$ results in the appearance of an IR band at 2192 cm^{-1} and a shoulder at 2167 cm^{-1} (Fig. 7a) which can be ascribed to $Mn^{2+}(CO)$ carbonyl species [35]. The removal of the CO gas phase and evacuation at ambient temperature leads to the disappearance of both bands.

CO adsorption on the evacuated $(Cu)_p(Mn)_pLSF$ sample results in the appearance of both low and high intensity IR bands (Fig. 7b). The main IR—CO band at 2145 cm^{-1} can be ascribed to $Cu^{2+}(CO)$ carbonyl species, whereas the band at 2074 cm^{-1} and the shoulder at 2110 cm^{-1} – to CO adsorbed on Cu^+ sites located in different cationic positions of the zeolite framework [36–38]. The partial reduction of Cu^{2+} to the Cu^+ state is a typical effect for CO chemisorption over copper oxides and Cu^{2+}-exchanged zeolites [36].

The removal of the CO gas phase and evacuation at ambient and elevated temperatures lead to disappearance of the first band assigned to the $Cu^+(CO)$ linear complexes and to a gradual decrease of intensity of the band that belongs to the $Cu^{2+}(CO)$ monocarbonyl species. As it was observed earlier for ZnLSF and $(Zn)_pLSF$ catalysts, the band of adsorbed CO_2 at 2355 cm^{-1} makes its appearance in the spectra for both Mn-containing catalysts only after letting air into the samples (Fig. 7).

Thus, the obtained DRIFT study results demonstrate that the Eley–Rideal mechanism of CO oxidation, which was attributed above to $(Cu)_p(Mn)_pLSF$ (see Section 3.4), is also characteristic for the single TrM exchanged faujasites ZnLSF, $(Zn)_pLSF$, and $(Mn)_pLSF$. CO interaction with TrM cations resulting in the formation of TrM mono- and dicarbonyls with the following conversion of the latter by oxygen into TrM carbonates–bicarbonates [39,40] is likely the reaction rate limiting step that in turn causes the relatively low activity of the mentioned catalysts at low temperature (see Table 2).

Completely different pictures are presented by the DRIFT spectra of chemisorbed CO on the $(Cu)_pCaLSF$ and $(Cu)_p(Zn)_pLSF$-2 catalysts (Figs. 8 and 9). An intense band at 2145 cm^{-1} and two shoulders near 2087 and 2165 cm^{-1} emerge in the $(Cu)_pCaLSF$ spectrum right after CO adsorption. These bands are related to the valent vibrations in the CO molecule adsorbed on Cu^{2+} and Cu^+ cations in the form of mono- and dicarbonyls respectively. As this takes place, an extended exposure of the sample in a CO atmosphere leads to the disappearance both the shoulders at 2087 and near 2165 cm^{-1} that is particular to dicarbonyl.

Meanwhile, the most distinguishing feature of this Cu polycation containing catalyst pertains to the occurrence and elevation of the band of stretching vibrations in CO_2 molecule at 2357 cm^{-1} after sample exposure in a CO atmosphere. What is more, letting air into the ampoule with the sample does not produce visible changes in the spectrum neither immediately after air admission, nor over 17 h long exposure in air.

It should be emphasized that a similar phenomenon was evident in [41,42] for other catalytic systems and it was considered as a direct confirmation of the Mars–van Krevelen model of CO oxidation. Indeed, the kinetics of CO oxidation by the $(Cu)_p$CaLSF catalyst, as it was pointed out above in Section 3.4, also speaks in favor of this mechanism.

In the case of the $(Cu)_p(Zn)_p$LSF-2 catalyst, as it follows from Fig. 9, the number of cation locations is smaller than what appears in the spectrum of $(Cu)_p$CaLSF (Fig. 8). There are two bands at 2140 cm^{-1} that has to be attributed to Cu^{2+} carbonyls formation and in the form of a shoulder near 2172 cm^{-1} which most likely relates to Zn^{2+} carbonyls. The characteristic peculiarity of this catalyst is that the band of adsorbed carbon dioxide at 2353 cm^{-1} emerges in the spectrum practically immediately after CO contacts the sample with the steady increase of the CO_2 yield over 68 h exposure of the sample in CO airless environment. Once again, air addition to the ampoule with the sample does not produce any changes in the spectrum. Thus, $(Cu)_p$CaLSF and $(Cu)_p(Zn)_p$LSF-2 are capable of performing CO oxidation without oxygen, in oxygen-free atmosphere.

Meanwhile, a rapid CO interaction with the catalyst, practically not involving an induction period (Fig. 9), and unusually high CO oxidation rates (Table 2) along with the zero order reaction kinetics for both reactants CO and O_2 (Fig. 5) suggest that in the case of the $(Cu)_p(Zn)_p$LSF-2 catalyst, an autocatalytic model of CO oxidation takes place, very similar to one that the authors [43] have found for Pd/Al_2O_3 containing substoichiometric Pd oxides.

In fact, oxygen atoms in super- and substoichiometric $[TrM_\alpha O_\beta]^{n+}$ polycations are exceptionally mobile and active, which allowed TrM polycation exchanged faujasites to perform mercaptan oxidation [11] and butadiene dimerization [13] without spontaneous involvement of free oxygen.

Accordingly, the real possibility of such an unconventional autocatalytic mechanism of CO oxidation can be verified by means of a continuous dynamic test for CO removal from an airless gas flow. With the purpose at hand, a tube reactor loaded with 10 cm^3 of the $(Cu)_p(Zn)_p$LSF-2 catalyst was used. Helium with a CO concentration of 0.1% vol. was fed into the reactor with a flow rate of 1 l/min. The CO breakthrough concentration was put on the level of 10 ppm and was registered by a gas chromatograph. In so doing, the time before CO breakthrough comprised 27 min, which defines the catalyst adsorption capacity on a quite commercially tolerable level of 0.41% w.

In such a manner, polycation exchanged faujasite $(Cu)_p(Zn)_p$LSF-2 can work not only as a CO oxidation catalyst but also as a chemisorbent for CO removal from oxygen free media.

The role of Zn polycations and their 1:2 proportion to Cu polycations in giving rise to the autocatalytic activity of the $(Cu)_p(Zn)_p$LSF-2 catalyst will be revealed in a consequent study.

4. Conclusions

Transition metal polycation exchanged LSF have been found to have a remarkable activity in the CO oxidation reaction, significantly exceeding the conventional catalysts performance at low temperatures. ESR and DRIFT spectroscopy suggest that transition metal polycation nanoclusters, particularly Cu and CuZn blended polycation clusters make the primary contribution to such outstanding catalytic activity. The research also shows that, depending on the TrM polycations composition, CO oxidation may proceed through various mechanisms and be governed by different kinetic laws. The most active CuZn polycations containing catalyst with the Cu:Zn = 2 cation ratio demonstrates an autocatalytic mechanism of CO oxidation with the zero order of the reaction rate for both components, CO and O_2. This offers a practical way for CO removal from oxygen free media.

Acknowledgement

The financial support from Russian Science Foundation (grant No. 14-50-00126) is acknowledged.

References

[1] M. Haruta, J. New Mater. Electrochem. Syst. 7 (2004) 163–172.
[2] A. Manaship, E. Gulari, Appl. Catal. B 37 (2002) 17–25.
[3] G. Dong, J. Wang, Y. Gao, S. Chen, Catal. Lett. 58 (1999) 37–41.
[4] Z.-Y. Pu, X.-S. Liu, A.-P. Jia, Y.-L. Xie, J.Q. Lu, M.-F. Luo, J. Phys. Chem. C 112 (2008) 15045–15051.
[5] N.A. Davshan, A.L. Kustov, O.P. Tkachenko, L.M. Kustov, C.H. Kim, ChemCatchem 7 (2014) 1990–1997.
[6] L. Heo, M.H. Wiebenga, J.R. Gaudet, I.S. Nam, L. Wei, Appl. Catal. B 160 (2014) 365–373.
[7] F. Ritter, A. Seidel, B. Boddenberg, Micropor. Mesopor. Mater. 24 (1998) 121–131.
[8] P.A. Anderson, Ionic clusters in zeolites, in: T.H.G. Karge, J. Weitcamp (Eds.), Molecular Sieves – Science and Technology. Post-Synthesis Modification, Springer, Berlin, 2002, p. 308.
[9] J. Livage, Catal. Today 41 (1998) 3–19.
[10] A. M. Tsybulevski, E.J. Rode, E.J. Weston, K.C. Weston, US Patent 6096,194, 2000.
[11] A. M. Tsybulevski, E.J. Rode, US Patent Application 9,404 A1, 2002.
[12] R.R. Shiriyazdanov, U. Sh Rysaev, S.A. Akhmetov, A.F. Morosov, E.A. Nikolaev, Petrol. Chem. 49 (2009) 86–89.
[13] A.M. Tsybulevski, L.M. Kustov, K.C. Weston, A.A. Greish, O.P. Tkachenko, A.V. Kucherov, Ind. Eng. Chem. Res. 51 (2012) 7073–7080.
[14] A. Martinez-Arias, D. Gamarra, M. Fernandes-Garcia, X.Q. Wang, J.C. Hanson, J.A. Rodrigez, J. Catal. 240 (2006) 1–7.
[15] X. Wang, J. Hanson, A.I. Frenkel, J.-M. King, J.A. Rodrigez, J. Phys. Chem. B 108 (2004) 13667–13673.
[16] B.R. Goodman, W.F. Schneider, K.C. Hass, J.B. Adams, Catal. Lett. 56 (1999) 183–188.
[17] W. Liu, M. Flytzani-Stephanopoulos, Chem. Eng. J. 64 (1996) 283–294.
[18] G. Sedmak, S. Hocevar, J. Levec, Top. Catal. 30/31 (2004) 445–451.
[19] A. M. Tsybulevski, A., Greish, L.M. Kustov, US Patent Appl. 20080194902, 2008.
[20] R.P. Townsend, E.N. Coker, Introduction to Zeolite Science and Practice, in: H. van Bekkum, E.M. Flanigen, P.A. Jacobs, J.C. Jansen (Eds.), 2nd ed., Elsevier, Amsterdam, 2001, p. 467.
[21] J.R. Anderson, K.C.L. Pratt, Introduction to Characterization and Testing of Catalysts, AP, New York, 1985.
[22] P. Kubelka, F. Munk, Z. Tech. Phys. 12 (1931) 593–601.
[23] P. Kubelka, J. Opt. Soc. Am. 38 (1948) 448–457, 44 1954, 330–335.
[24] H. Falsig, B. Hvolbaek, I.S. Kristensen, T. Jiang, T. Bligard, C.H. Christensen, J.K. Norskov, Angew. Chem. 120 (2008) 4840–4844.
[25] D.M. Whittle, A.A. Mirzaei, J.S.J. Hargreeves, R.W. Joyner, C.J. Kiely, S.H. Taylor, G.J. Hatchings, Phys. Chem. Chem. Phys. 4 (2002) 5915–5920.
[26] M. Haruta, S. Tsubota, T. Kobayashi, M.J. Gonet, B. Delmon, J. Catal. 144 (1993) 175–192.
[27] P. Mars, D.W. van Krevelen, Chem. Eng. Sci. 3 (1954) 41–44.
[28] K. Morgan, K.J. Cole, A. Goguet, C. Hardacre, G.J. Hutchings, N. Maguire, S.H. Taylor, J. Catal. 276 (2010) 38–48.
[29] J.-Q. Lu, C.-X. Sun, N. Li, A.-P. Jia, M.-F. Luo, Appl. Surf. Sci. 287 (2013) 124–134.
[30] C. Bürgel, N.M. Reilly, C.E. Johnson, R. Mitrich, M.L. Kimble, A.W. Castleman, V. Banacic-Kontecky, J. Am. Chem. Soc. 130 (2008) 1694–1698.
[31] N.P. Lebedeva, M.T. Koper, J.M. Feliu, R.A. van Santen, J. Electroanal. Chem. 242 (2002) 524–525.
[32] X.-N. Li, Z. Yuan, S.-G. He, J. Am. Chem. Soc. 136 (2014) 3617–3623.
[33] G. Djega-Mariadassou, M. Boudart, J. Catal. 216 (2003) 89–97.
[34] S. Bordiga, E. Garrone, C. Lamberti, A. Zecchina, C. Arean, V.B. Kazansky, L.M. Kustov, J. Chem. Soc. Faraday Trans. 90 (21) (1994) 3367–3372.
[35] K.I. Hadjivanov, G.N. Vasilev, Adv. Catal. 47 (2002) 307–511.
[36] A.A. Davydov, Molecular Spectroscopy of Oxide Catalyst Surfaces, Willey, London, 2003.
[37] V.Y. Borovkov, H.G. Karge, J. Chem. Soc. Faraday Trans. 91 (1995) 2035–2039.
[38] A.A. Davydov, Kinet. Catal. 26 (1985) 135–167.
[39] B.-Z. Sun, W.-K. Chen, Y.-J. Xu, J. Chem. Phys. 133 (2010) 154502–154509.

[40] D.A. Svintsitskiy, A.P. Chupakin, E.M. Slavinskaya, O.A. Stonkus, A.I. Stadnichenko, S.V. Koscheev, A.I. Boronin, J. Mol. Catal. A: Chem. 368–369 (2013) 95–106.
[41] V.M. Rakic, R.V. Hercigonja, V.T. Dondur, Micropor. Mesopor. Mater. 27 (1999) 27–39.
[42] V. Iablokov, K. Frey, O. Geszti, N. Kruse, Catal. Lett. 134 (2010) 210–216.
[43] K. Zorn, S. Giorgio, E. Halwax, C.R. Henry, H. Grönbeck, G. Rupprechter, J. Phys. Chem. C 115 (2011) 1103–1111.